Analyst

PAPER

View Article Online
View Journal

Cite this: DOI: 10.1039/d5an01339a

Multi-modal structure characterization of synthetic batch impurities with liquid chromatography coupled to infrared ion spectroscopy

Teun van Wieringen, [a,b] Simon J. Perry, [c] Agisilaos Chantzis, [c] Giel Berden, [a,b] Jos Oomens, [a,b] Mansoor Saeed [c] and Jonathan Martens *[a,b]

Assessing the safety of agrochemical products requires a thorough structural identification of synthetic batch impurities. The traditional method, relying on liquid chromatography paired with high-resolution tandem mass spectrometry, is often insufficient for complete structural determinations. Infrared ion spectroscopy has emerged as a novel analytical approach for structural characterisation in mass spectrometry. This technique integrates infrared spectroscopy with mass spectrometry and obtains infrared spectra of mass-isolated ions within the spectrometer and can be combined with liquid-chromatography separation methods. The infrared spectral patterns provide unique fingerprints for molecules with identical masses but different structures, and can be predicted through quantum chemistry, eliminating the need for reference standards. We demonstrate this methodology's application in analysing agrochemical batch impurities by successfully identifying five impurity structures, including two previously undocumented compounds that are identified based on the match to their computed spectra. Additionally, we showcase the detection and structural determination of a trace impurity that undergoes reconversion to the parent active compound. Here, Born–Oppenheimer molecular dynamics calculations are used to predict and assign the infrared spectrum, describing the experimental broadened absorption line shapes resulting from hydrogen bonding.

Received 18th December 2025,
Accepted 26th April 2026

DOI: 10.1039/d5an01339a

rsc.li/analyst

Introduction

During the synthesis of a chemical, by-products may arise, contaminating the final batch. In the agrochemical industry, these impurities may have the potential to lead to toxicological effects or contamination of the environment.[1] Therefore, regulatory bodies have set strict regulations regarding the impurity profiling of new active substances in different sectors within the chemical industry. Completely removing organic impurities arising in a multistep synthesis is typically difficult or costly. For agrochemicals[2] and pharmaceuticals,[3] all components with apparent levels higher than 0.1% of the main product should be characterised and assessed for safety. Essential to this process is the structural identification of the impurities.

Impurities are commonly detected and quantified (relatively) using liquid chromatography (LC), usually combined with mass spectrometry (MS).[4] Advances in analytical chemistry, and specifically LC-MS (*e.g.* column technology[5]) and mass spectrometry developments,[6] have enabled the identification of very minor components directly from complex sample matrices.[7] In recent years, the increased access to high-resolution accurate mass (HRAM) spectrometers[8–10] has improved the ability to determine molecular formulas; however, difficulties in determining chemical structures remain. The structural information obtained from fragmentation mass spectrometry (MS/MS) is often insufficient for a complete structural determination. On the other hand, when a significant amount of the impurity (>100 μg) can be isolated in pure form, nuclear magnetic resonance (NMR) commonly gives direct insight into the analyte's structure.[11,12] However, as the impurities are generally present in low amounts, the isolation of enough material for NMR can be a costly and laborious task. In this work, we demonstrate how infrared ion spectroscopy (IRIS) is used to determine the structure of agrochemical batch impurities.

IRIS combines structural information from infrared (IR) spectroscopy with the sensitivity and selectivity gained from MS by

[a]HFML-FELIX, Toernooiveld 7, Nijmegen, 6525 ED, The Netherlands. E-mail: jonathan.martens@ru.nl
[b]Institute for Molecules and Materials, Radboud University, Heyendaalseweg 135, Nijmegen, 6525 AJ, The Netherlands
[c]Syngenta, Jealott's Hill International Research Centre, RG42 6EY Bracknell, Berkshire, UK

measuring the IR spectrum of the mass-isolated ion population directly in an ion-trapping mass spectrometer. The technique has previously been shown to be effective for identifying metabolites,[13–15] agrochemical derivatives,[16,17] micro-pollutants,[18] and impurities in organic electronic materials.[19] The technique can be combined with the common workflows used for impurity characterisation based on LC-MS.[20] Quantum-chemical methods, notably density functional theory (DFT), are able to accurately predict the IR spectrum[21] and provide confidence for synthesising the correct compound, preventing the unnecessary synthesis of candidates that do not match; in some cases, a synthetic standard may not be necessary at all.

In this work, we describe the impurity profiling of a novel fungicide having a substituted oxadiazole. The active ingredient (main product in Scheme 1) is synthesised from *p*-tolunitrile in five steps, of which the last two steps, forming the oxadiazole, are shown.[22,23] To protect proprietary structural information related to compounds currently under patent and in development, the R-group is not further specified but is the same for all intermediates and impurities shown. The chemical transformations generating the impurities occur exclusively on the side of the molecule that is shown, thereby enabling explanation of the formation chemistry while safeguarding confidential intellectual property. During each of the steps, side products can be formed, or residual reactants can be carried over to the final batch. The oxadiazole is an important structural motif in medicinal and agrochemistry and the identified impurities could potentially arise in active ingredients produced *via* a similar synthetic route.[24]

We have obtained two stable reaction intermediates as reference materials and used LC-MS to confirm their presence and detected new impurities present in the synthetic batch. We used IRIS to structurally characterise all impurities. The final structural assignments are made by comparing the IRIS fingerprint of the unknowns with quantum-chemically predicted spectra and reference standards when available.

Methods

Materials

LC-MS grade water, methanol, acetonitrile and formic acid were obtained from Merck (Darmstadt, Germany). Samples and reference compounds were obtained from Syngenta (Münchwilen, Switzerland).

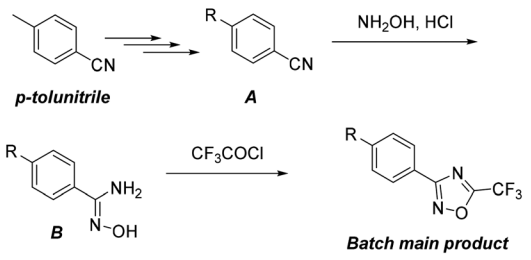

Scheme 1 Synthetic scheme for the synthesis of the main batch component. The R group is the same for the shown structures.

Sample preparation

Samples were prepared from the batch at a concentration of 1 mg mL^{-1} in acetonitrile and subsequently diluted to 100 μg mL^{-1} in water.

Liquid chromatography

A chromatographic method was adapted from ref. 25. Aliquots of 2 μL were injected into a Waters Acquity UPLC HSS T3 100 Å (2.1 × 100 mm, 1.8 μm) reversed-phase column. For the injection and gradient, a Bruker Elute UPLC system, equipped with a column oven and autosampler, was used. The system is coupled to a Bruker AmaZon quadrupole ion trap mass spectrometer operating in positive ESI mode. Eluent A consists of water with 0.1% formic acid and eluent B consists of methanol with 0.1% formic acid. We used the following elution program: 0–1 min, 0% B; 1–16 min, 0–100% B; 16–20 min, 100% B; 20–21 min, 100%–0% B; 21–25 min, 0% B (flow: 0.4 mL min^{-1}).

The asymmetry factor is determined by dividing the half-width after the maximum by the half-width before the maximum. The half-widths are determined at 10% of the peak height.

Infrared ion spectroscopy

Spectroscopic experiments are carried out on the Bruker AmaZon ion trap mass spectrometer, which has been modified as described in detail previously[26] and is coupled to the FELIX infrared free-electron laser. Fractions were manually collected from the LC system in vials at the retention times determined in a previous injection and stored overnight at 5 °C before spectroscopic analysis or collected in a 60 μL sample loop using online heartcutting.[20] The fractions are introduced to the electrospray ionisation source using a syringe pump at a flow rate of 2 μL min^{-1}. IRIS experiments are conducted by recording mass spectra while scanning the laser frequency over the 750–1850 cm^{-1} spectral range in steps of 3–5 cm^{-1}, as described previously.[26] The frequency-dependent IR photodissociation yield is then used to reconstruct an IR spectrum, which is corrected for wavelength-dependent power variations of the FELIX laser and normalised to the highest intensity peak.

High-resolution mass spectrometry

High-resolution mass spectrometry experiments are conducted on a Fourier transform ion cyclotron resonance mass spectrometer[27] (FTICR, SolariX XR 7T, Bruker Daltonik, Bremen, Germany) coupled to the chromatography setup described above and operated in positive ESI mode.

Quantum-chemical calculations

IR spectra are predicted using quantum chemistry methods starting from the 2D representation of the candidate structure in SMILES notation, using a method adapted from the workflow previously described.[21] Tautomers and protonation isomers were created using RDKIT,[28] after which conformers

were generated for each isomer using CREST v.2.12[29] employing the GFN2-xTB[30] method. CREST is used to cluster the conformers found for each protonation tautomer using the default settings. Conformers were selected up to 60 kJ mol^{-1} based on their GFN2-xTB energy and further optimised at the BP86/def2-SV(P)[31–34] level using ORCA v.6.0.1,[35] followed by a harmonic frequency calculation to obtain the free energy. After filtering on the relative free energy (up to 25 kJ mol^{-1}), the conformers were further optimised at the B3LYP/ma-def2-SVP[36,37] level, followed by a harmonic frequency calculation and a single point DLPNO-MP2/def2-TZVP[38] calculation. The MP2 energy is combined with the B3LYP thermal energy to give the free energy, used as a final ranking. The B3LYP frequencies are scaled by 0.975 and 0.955 for frequencies below and above 2500 cm^{-1}, respectively,[39,40] and the vibrational stick spectra are convoluted by a Gaussian broadening function with a full-width-half-maximum of 20 cm^{-1} to facilitate comparison with the experimental spectrum.

Similarity scores (S), ranging from 0 to 1000, are calculated as cosine similarity between the measured and predicted spectra in the frequency range from 700 to 1900 cm^{-1}.[21] Both spectra are normalised to the highest intensity peak and their intensities are transformed by taking the square root to reduce the influence of band intensities on the score and hence increase that of the spectral positions. The similarity score is defined as $S = 1000\sqrt{A} \cdot \sqrt{B}/\left(\left|\sqrt{A}\right| \cdot \left|\sqrt{B}\right|\right)$, in which A and B are vectors containing the normalised spectral intensities. A score closer to 1000 indicates greater similarity.

Born–Oppenheimer molecular dynamics calculations are performed using Turbomole[41] 7.8 and the r^{2}scan-D4/def2-SVP density functional method using a method adapted from ref. 42. Four independent Molecular Dynamics (MD) runs are conducted with the same starting geometry but different random initial velocities matching a kinetic temperature of 250 K. A timestep of 20 a.u. (~0.48 fs) and a Nosé–Hoover thermostat of 350 K,[43] with a time coupling constant of 400 a.u., are used to perform 45 000 MD steps. Drift of and rotation around the centre of mass are removed after each subsequent 56 steps. The molecular electric dipole moment, as calculated with DFT, is written to a file at each step. The first 5000 steps are used to equilibrate the system and the remaining 40 000 steps are used to calculate the IR spectrum using the Fourier transform of the autocorrelation function of the electric dipoles by the TRAVIS[44] software package. The four computed IR spectra are averaged to yield the final spectrum. To correct for systematic errors in the method, the frequencies are scaled[43] by 0.980 and 0.955 in the region below and above 2500 cm^{-1}, respectively. Developed for liquids, most BOMD calculations for spectral prediction make use of periodic calculations, with plane wave basis DFT.[45] The definition of a dipole in these periodic systems is not trivial and different solutions have been developed to obtain the dipole.[46,47] The current BOMD calculation, however, is done using atom-centred basis sets, which are particularly suitable for gas-phase calculations. In this case, the dipole is easily obtained from the charge density, calculated in density functional theory.

Results and discussion

Detection of impurities

Fig. 1 presents the LC chromatogram of the batch sample, showing the separation of the impurities and their detection with LC-MS. Besides the main product peak, eluting at 13.42 minutes, five impurity peaks are observed, labelled **1–5**. The impurities are well separated during chromatography. Impurity **1** is identified as the unreacted amidoxime intermediate (**B** in Scheme 1) and matches the m/z and retention time of the reference material. Impurity **3** matches in m/z and retention time to reference material of the nitrile intermediate (**A** in Scheme 1). The nominal mass of impurity **2** matches with that of a known side product in the formation of the *N*-hydroxyl amidine,[48] in which the nitrile is hydrolysed to an amide. Impurities **4** and **5** were previously unknown.

Relative quantification was done by integration of Gaussians fitted to the extracted ion chromatogram of the protonated ions (SI Fig. S1). Retention times and relative abundances are shown in Table 1. All impurities found have an abundance of more than 0.1%, so they require identification according to standard regulations. The ion intensity of the lowest-intensity feature is three times higher than the background signal, indicating that this is close to the limit of detection (LOD) of this method (based on a LOD of 3 : 1 S/N). For a higher sensitivity, a larger injection volume or concentration can be used at the risk of overloading the column. Furthermore, the peak of the main product is tailing (see also fitted Gaussian in Fig. S1, asymmetry factor 1.29). An impurity that coelutes or elutes later than the main product could be overshadowed by the main ingredient.

Impurity identification

The IRIS spectra of the impurities are measured by direct infusion of the collected fractions and mass isolation of the corresponding m/z value in the ion trap; they are shown as the black traces in Fig. 2. For impurities **1** and **3**, reference standards are

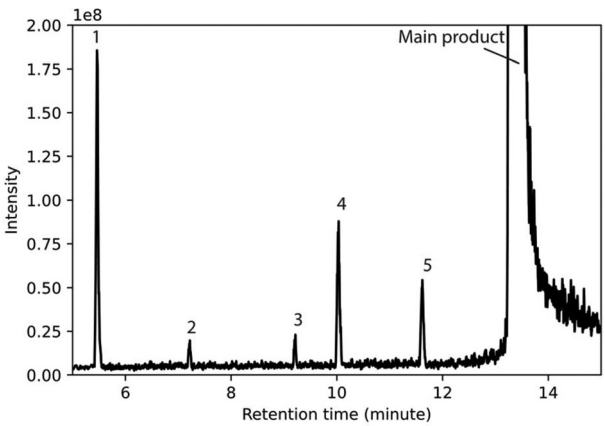

Fig. 1 Base Peak Chromatogram for the separation of the batch sample. The main product elutes at 13.42 min, 5 different impurities are observed, indicated (**1–5**), eluting earlier than the main ingredient.

Table 1 Overview of detected compounds

Compound	m/z $[M + H]^+$	Retention time (min)	Apparent relative abundance (%)
Impurity **1**	282	5.46	1.91
Impurity **2**	267	7.24	0.24
Impurity **3**	249	9.26	0.26
Impurity **4**	378	10.09	1.16
Impurity **5**	350	11.70	0.75
Main product	360	13.42	95.7

available and their IRIS spectra are shown as grey shades in Fig. 2A and C.

The IR spectrum of the protonated impurity **1** has its most intense band at 1653 cm^{-1}, resulting from the CN stretch of the *N*-hydroxyl amidine.[49] Furthermore, a carbonyl stretch at 1698 cm^{-1} can be observed. In the spectrum measured from the impurity, these bands overlap, while a shoulder can be observed in the spectrum of the reference molecule. The differences can be attributed to the small day-to-day fluctuations in spectral broadness and power profile of the FEL radiation. A similar comparison can be made for impurity **3**, shown in Fig. 2C. The peak positions and relative intensities match closely between the spectrum from the impurity and the reference standard. Similarity scores are able to uniquely identify impurities **1** and **3** based on their match to the reference material spectra (Table S1).

In the absence of standards, tentative assignments are supported by quantum chemically computed IR spectra (shown as blue-shaded spectra in Fig. 2). For impurities **1** and **3**, they show a good match to the experimental spectra over the full spectral range. Hence, we conclude that the level of theory is sufficient to reliably predict the IR spectra for these molecules. Although impurity **2** was previously assigned using LC, we did not have access to a reference standard. To confirm the identification, the experimental IR spectrum was compared to the computationally predicted spectrum, which again shows good alignment, whereas an alternative aldoxime candidate (Fig. S2) displays a poorer fit, further supporting the assignment.

Impurity **5** does not match any of the reactants or known impurities from the reaction. We determined the molecular formula based on the accurate mass from high-resolution mass spectrometry (Fig. S3) and propose the chemical structure shown in Fig. 2F. It has a 2-methoxypropanoyl group and is expected to be formed by a reaction of 2-methoxypropanoyl chloride with the amidoxime[50] (**B** in Scheme 1), when traces of it are present in the reaction mixture. The IR spectrum of this structure is predicted using quantum chemistry and matches closely with that measured for impurity **5** (Fig. 2F). Furthermore, a comparison with an alternative isopropoxy derivative (Fig. S4) yielded inferior agreement and a lower similarity score, giving strength to the assignment.

Impurity **4** has an m/z that is 18 units higher than the main product and likely results from the addition of water. After

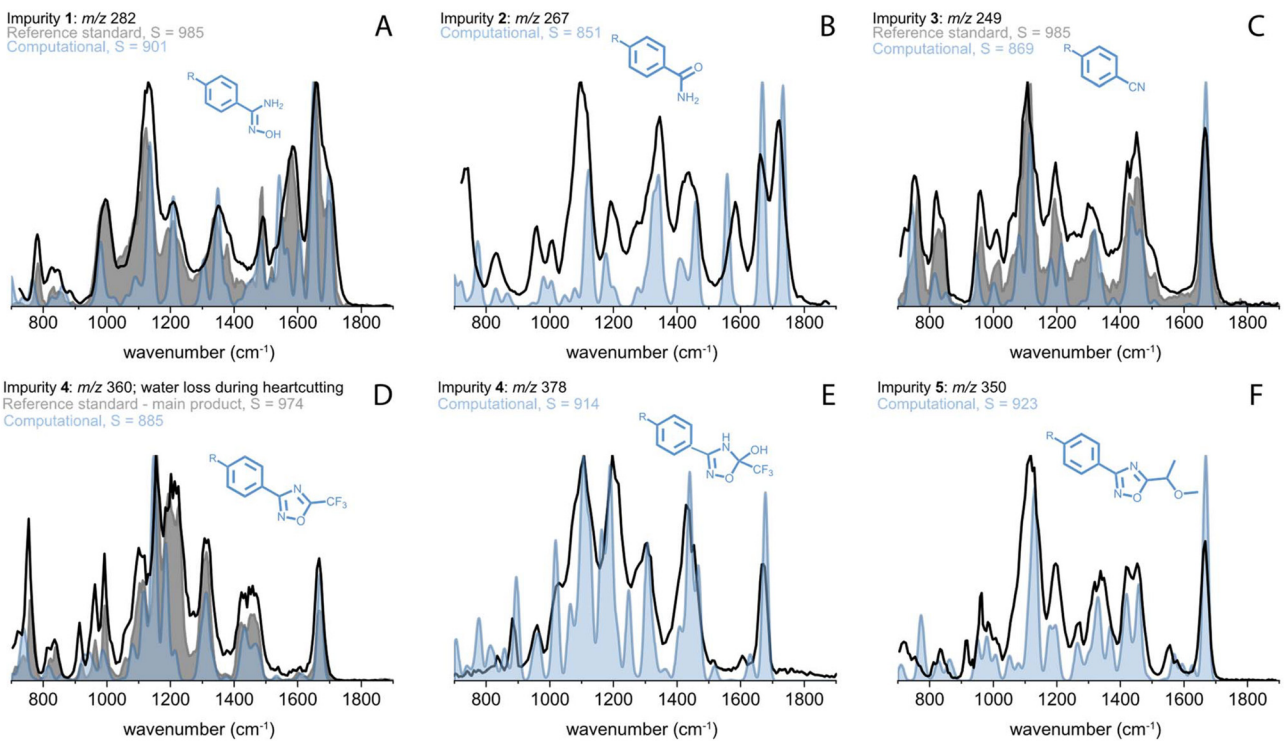

Fig. 2 Black trace: experimental IR spectra from impurities **1**, **2**, **3**, **4** after water loss, **4**, and **5** in panel A to F, respectively. Gray shaded traces: IRIS spectrum of reference standard, when available. Blue shaded traces: predicted IR spectrum for the shown structure using density functional theory. The R-group is the same for all calculated structures. Spectral similarity scores (*S*) are calculated to evaluate the match to the impurity spectra.

fractionation, it reconverted to a compound with the *m*/*z* of the main product when stored overnight. As can be observed in Fig. 2D, the IRIS spectrum of this dehydrated product of impurity **4** matches that of the main product, confirming that it is reformed overnight. The calculated spectrum does not fully explain the band at 1185–1230 cm^{-1}. The calculated band at 1185 cm^{-1} corresponds to a C–F stretch vibrational mode, which is known to be predicted at a too low frequency by our DFT method.[16]

The storage time of the fraction can be reduced using an on-line heartcutting LC-MS approach,[20] which allows us to record the IRIS spectrum of impurity **4**. Harmonic IR spectra of three candidate structures in which the oxadiazole ring is hydrated are predicted using DFT. In candidate **4a**, the ring is hydrated to a dihydrooxadiazol-5-ol, in candidate **4b** the ring is hydrolysed to an *N*-acyl,*N*′-hydroxy-carbamimidoyl, while for candidate **4c** it is hydrolysed to an *O*-acylamidoxime. All three structural motifs and their reaction to the main product are described in the literature.[51–53] The structural motif of isomer **4a** has been isolated before, and a slow dehydration at room temperature has been described.[53] The calculated spectrum for candidate **4a** shows the best match to the experimental spectrum (Fig. 3), based on visual inspection and the similarity score. The absence of a vibrational band between 1700 and 1850 cm^{-1} is particularly diagnostic and indicates that there is no free carbonyl group in an amide or ester, suggesting that the oxadiazole ring is intact. The higher frequency range, where the OH and NH stretches are present, provides extra confidence in the assignment. The absence of the primary amine NH_2 stretch and the presence of a free OH stretch (in addition to the single carbonyl stretch) confirm the assignment. We observe a broad feature roughly between 2800 and 3400 cm^{-1}, which is due to an intermolecular hydrogen bond from the protonated site. The harmonic approximation is not able to accurately describe the dynamic behaviour of hydrogen bonds. BOMD calculations have been shown to be able to accurately describe these dynamics and provide better spectral predictions for such systems.[42,43] Fig. 3 shows agreement with the experimental IR spectrum, including the broadened profile of the proton stretching mode.[54,55] Not only does the high-frequency range match better, but also in the lower frequency range, the BOMD calculations closely predict the broadness of the spectral features, while the harmonic frequency calculations are simply convolved with a uniform Gaussian line-broadening function. The BOMD spectra show a similar quality match as the reference standards, and therefore provide additional confidence in the assignment over the harmonic spectral predictions when reference materials are not available.

As impurity **4** converts to the main ingredient, it is expected to be in equilibrium with the main product, which can shift based on environmental conditions (pH, temperature, solvent) and can be formed during the analysis. We expect this type of hydration reaction to be common for other 1,2,4-oxadiazole-containing molecules and would likely alert impurity profiling analysts of this possibility, which may be incorrectly assigned as a contaminant. By applying heartcutting LC-MS, the fraction storage time was effectively reduced to measure the IRIS spectrum of impurity **4** in its original state before observing significant reconversion to the dehydrated form.

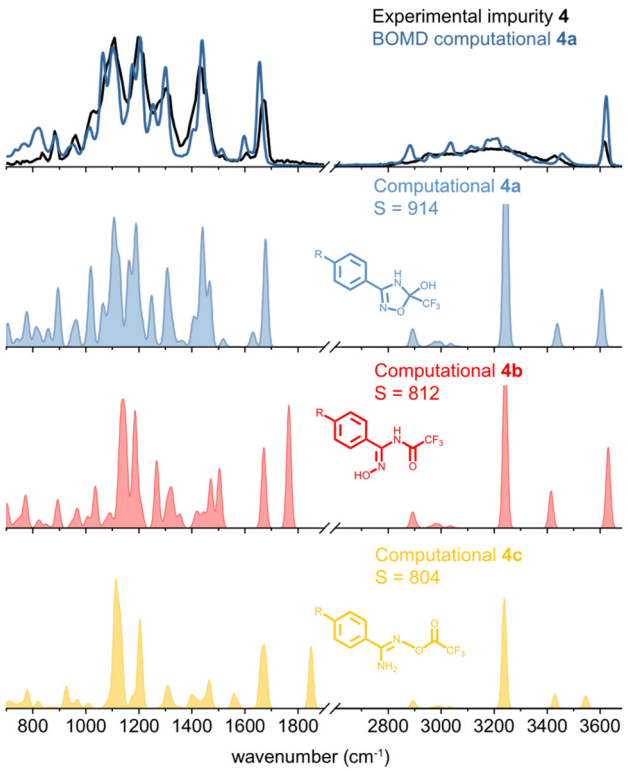

Fig. 3 Comparison of the spectrum of impurity **4** (black trace) to predicted spectra (colored). Harmonic DFT predicted spectra (colored filled curves) are shown for three candidates with their similarity scores (*S*) for the match to the experimental spectrum. Isomer **4a** (blue) shows the best match to the experimental spectrum. The BOMD calculation (blue trace in upper panel) improves the match as compared to the harmonic frequency and correctly predicts the broadening of the peaks. The R group is the same for all candidates.

Conclusions

We successfully identified and characterised five impurities, including two previously unknown compounds through a multi-modal analytical approach effectively combining chromatography and IR ion spectroscopy. The structural assignment can be made by a direct comparison of IRIS spectra to those of reference standards or to quantum-chemical computational predictions, when reference standards are unavailable. Here, BOMD IR spectral predictions give more confidence to the match as they predict the broadness explicitly. While traditional methods like NMR require substantial sample quantities and time-consuming isolation procedures, IRIS demonstrated superior capability in analysing ultra-low abundance synthetic impurities directly from chromatographic separations.

The characterisation of five impurities, ranging from reaction intermediates and literature described impurities to a fully novel 1,2,4-oxadiazole water addition product, proves the applicability in an industrial environment. A critical step in the reference-free structure assignment remains the initial formation of candidate structures, where chemical intuition and complementary analytical data (HRAM, MS/MS) remain very valuable.

Looking forward, this analytical method offers an efficient pathway for impurity profiling in agrochemical and pharmaceutical chemistry, potentially accelerating development and giving more confidence to the structural assignments.

Author information

TvW: investigation, visualization, writing – original draft. SJP: conceptualization, investigation, writing – review & editing. AC: conceptualization, investigation, writing – review & editing. JO: writing – review & editing. GB: writing – review & editing. MS: conceptualization, investigation, writing – review & editing. JM: conceptualization, investigation, writing – review & editing.

Conflicts of interest

There are no conflicts to declare.

Data availability

All data can be obtained from the corresponding author upon reasonable request.

Supplementary information (SI): extracted ion chromatograms for the impurities and main product including Gaussian fits, similarity scores, alternative calculations, high-resolution mass spectra, and MS/MS spectra. See DOI: https://doi.org/10.1039/d5an01339a.

Acknowledgements

The authors gratefully acknowledge the excellent technical assistance from the FELIX group. We thank the SURFsara Supercomputer Centre and the NWO ENW-domain for the computational resources (NWO Rekentijd Grant 2024.009) enabling the quantum-chemical calculations.

References

1 P. Maienfisch, *Adv. Agrochem*, 2022, **1**, 148–156.
2 European commision, Guidance document on the assessment of the equivalence of technical materials of substances regulated under regulation (EC) No 1107/2009, 2012.
3 International Council for Harmonisation of Technical Requirements for Pharmaceuticals for Human Use, Impurities In New Drug Substances Q3A(R2), 2006.
4 J. Kannoujia, N. Chirra, R. Rodda, A. Shaikh, N. Maddala, S. Kantevari and P. Sripadi, *Rapid Commun. Mass Spectrom.*, 2024, **38**, e9729.
5 M. E. Swartz, *J. Liq. Chromatogr. Relat. Technol.*, 2005, **28**, 1253–1263.
6 C. Li, S. Chu, S. Tan, X. Yin, Y. Jiang, X. Dai, X. Gong, X. Fang and D. Tian, *Front. Chem.*, 2021, **9**, 813359.
7 R. Holm and D. P. Elder, *Eur. J. Pharm. Sci.*, 2016, **87**, 118–135.
8 S. J. Perry, S. Nász and M. Saeed, *Rapid Commun. Mass Spectrom.*, 2015, **29**, 1545–1555.
9 M. Zhu, L. Ma, D. Zhang, K. Ray, W. Zhao, W. G. Humphreys, G. Skiles, M. Sanders and H. Zhang, *Drug Metab. Dispos.*, 2006, **34**, 1722–1733.
10 P. H. Harlow, S. J. Perry, A. J. Stevens and A. J. Flemming, *Sci. Rep.*, 2018, **8**, 13333.
11 R. M. Maggio, N. L. Calvo, S. E. Vignaduzzo and T. S. Kaufman, *J. Pharm. Biomed. Anal.*, 2014, **101**, 102–122.
12 J. Lin, X. Zheng, D. Li, H. Hou, X. Chen, J. Jin, X. Zhang, W. Chen and M. Li, *Org. Process Res. Dev.*, 2024, **28**, 4407–4419.
13 A. Ben Faleh, S. Warnke, T. van Wieringen, A. H. Abikhodr and T. R. Rizzo, *Anal. Chem.*, 2023, **95**, 7118–7126.
14 R. E. van Outersterp, J. Martens, G. Berden, A. Lubin, F. Cuyckens and J. Oomens, *Chem.: Methods*, 2023, **3**, e202200068.
15 R. E. van Outersterp, K. J. Houthuijs, G. Berden, U. F. Engelke, L. A. J. Kluijtmans, R. A. Wevers, K. L. M. Coene, J. Oomens and J. Martens, *Int. J. Mass Spectrom.*, 2019, **443**, 77–85.
16 M. J. A. Vink, F. A. M. G. van Geenen, G. Berden, T. J. C. O'Riordan, P. W. A. Howe, J. Oomens, S. J. Perry and J. Martens, *Environ. Sci. Technol.*, 2022, **56**, 15563–15572.
17 M. J. A. Vink, J. J. Schermer, J. Martens, W. J. Buma, G. Berden and J. Oomens, *ACS Agric. Sci. Technol.*, 2023, **3**, 171–180.
18 K. J. Houthuijs, M. Horn, D. Vughs, J. Martens, A. M. Brunner, J. Oomens and G. Berden, *Chemosphere*, 2023, **341**, 140046.
19 H. Takano, D. Visser, L. van Tetering, T. van Wieringen, G. Berden, J. Oomens, D. Shirakura, H. Fujimoto, C. Adachi and K. Matsuda, *Anal. Chem.*, 2026, **98**, 7603–7612.
20 R. E. van Outersterp, J. Oosterhout, C. R. Gebhardt, G. Berden, U. F. H. Engelke, R. A. Wevers, F. Cuyckens, J. Oomens and J. Martens, *Anal. Chem.*, 2023, **95**, 3406–3413.
21 K. J. Houthuijs, G. Berden, U. F. H. Engelke, V. Gautam, D. S. Wishart, R. A. Wevers, J. Martens and J. Oomens, *Anal. Chem.*, 2023, **95**, 8998–9005.
22 S. Kitamura, H. Fukushi, T. Miyawaki, M. Kawamura, Z.-i. Terashita and T. Naka, *Chem. Pharm. Bull.*, 2001, **49**, 268–277.

23 N. S. Ooi and D. A. Wilson, *J. Chem. Soc., Perkin Trans. 2*, 1980, 1792–1799, DOI: 10.1039/P29800001792.
24 A. Vörös, Z. Baán, P. Mizsey and Z. Finta, *Org. Process Res. Dev.*, 2012, **16**, 1717–1726.
25 K. L. M. Coene, L. A. J. Kluijtmans, E. van der Heeft, U. F. H. Engelke, S. de Boer, B. Hoegen, H. J. T. Kwast, M. van de Vorst, M. C. D. G. Huigen, I. M. L. W. Keularts, M. F. Schreuder, C. D. M. van Karnebeek, S. B. Wortmann, M. C. de Vries, M. C. H. Janssen, C. Gilissen, J. Engel and R. A. Wevers, *J. Inherited Metab. Dis.*, 2018, **41**, 337–353.
26 J. Martens, G. Berden, C. R. Gebhardt and J. Oomens, *Rev. Sci. Instrum.*, 2016, **87**, 103108.
27 K. J. Houthuijs, L. van Tetering, J. L. Schuurman, C. A. Wootton, C. R. Gebhardt, M. E. Ridgeway, G. Berden, J. Martens and J. Oomens, *Int. J. Mass Spectrom.*, 2024, **505**, 117323.
28 RDKit: Open-source cheminformatics. https://www.rdkit.org.
29 P. Pracht, F. Bohle and S. Grimme, *Phys. Chem. Chem. Phys.*, 2020, **22**, 7169–7192.
30 C. Bannwarth, S. Ehlert and S. Grimme, *J. Chem. Theory Comput.*, 2019, **15**, 1652–1671.
31 A. D. Becke, *Phys. Rev. A*, 1988, **38**, 3098–3100.
32 J. P. Perdew, *Phys. Rev. B: Condens. Matter Mater. Phys.*, 1986, **33**, 8822–8824.
33 F. Weigend and R. Ahlrichs, *Phys. Chem. Chem. Phys.*, 2005, **7**, 3297–3305.
34 F. Weigend and R. Ahlrichs, *Phys. Chem. Chem. Phys.*, 2006, **8**, 1057–1065.
35 F. Neese, *Wiley Interdiscip. Rev.: Comput. Mol. Sci.*, 2025, **15**, e70019.
36 A. D. Becke, *J. Chem. Phys.*, 1993, **98**, 5648–5652.
37 J. Zheng, X. Xu and D. G. Truhlar, *Theor. Chem. Acc.*, 2011, **128**, 295–305.
38 P. Pinski, C. Riplinger, E. F. Valeev and F. Neese, *J. Chem. Phys.*, 2015, **143**, 034108.
39 A. P. Scott and L. Radom, *J. Phys. Chem.*, 1996, **100**, 16502–16513.
40 J. K. Martens, J. Grzetic, G. Berden and J. Oomens, *Int. J. Mass Spectrom.*, 2015, **377**, 179–187.
41 Y. J. Franzke, C. Holzer, J. H. Andersen, T. Begušić, F. Bruder, S. Coriani, F. Della Sala, E. Fabiano, D. A. Fedotov, S. Fürst, S. Gillhuber, R. Grotjahn, M. Kaupp, M. Kehry, M. Krstić, F. Mack, S. Majumdar, B. D. Nguyen, S. M. Parker, F. Pauly, A. Pausch, E. Perlt, G. S. Phun, A. Rajabi, D. Rappoport, B. Samal, T. Schrader, M. Sharma, E. Tapavicza, R. S. Treß, V. Voora, A. Wodyński, J. M. Yu, B. Zerulla, F. Furche, C. Hättig, M. Sierka, D. P. Tew and F. Weigend, *J. Chem. Theory Comput.*, 2023, **19**, 6859–6890.
42 T. van Wieringen, A. Lubin, R. van Outersterp, J. Martens, E. van Beelen, J. Oomens, F. Cuyckens and G. Berden, *Anal. Chem.*, 2025, **97**, 17216–17223.
43 B. Martínez-Haya, J. R. Avilés-Moreno, F. Gámez, J. Martens, J. Oomens and G. Berden, *Phys. Chem. Chem. Phys.*, 2024, **26**, 198–208.
44 M. Brehm, M. Thomas, S. Gehrke and B. Kirchner, *J. Chem. Phys.*, 2020, **152**, 164105.
45 M. Thomas, M. Brehm, R. Fligg, P. Vöhringer and B. Kirchner, *Phys. Chem. Chem. Phys.*, 2013, **15**, 6608–6622.
46 D. R. Galimberti, A. Milani, M. Tommasini, C. Castiglioni and M.-P. Gaigeot, *J. Chem. Theory Comput.*, 2017, **13**, 3802–3813.
47 M. Thomas, M. Brehm and B. Kirchner, *Phys. Chem. Chem. Phys.*, 2015, **17**, 3207–3213.
48 A. Vörös, Z. Mucsi, Z. Baán, G. Timári, I. Hermecz, P. Mizsey and Z. Finta, *Org. Biomol. Chem.*, 2014, **12**, 8036–8047.
49 A. M. Atta, H. A. Al-Lohedan and S. A. Al-Hussain, *Int. J. Mol. Sci.*, 2015, **16**, 6911–6931.
50 S. Chiou and H. J. Shine, *J. Heterocycl. Chem.*, 1989, **26**, 125–128.
51 H. Otaka, J. Ikeda, D. Tanaka and M. Tobe, *Tetrahedron Lett.*, 2014, **55**, 979–981.
52 Y.-I. Lin, S. A. Lang Jr, M. F. Lovell and N. A. Perkinson, *J. Org. Chem.*, 1979, **44**, 4160–4164.
53 A. R. Gangloff, J. Litvak, E. J. Shelton, D. Sperandio, V. R. Wang and K. D. Rice, *Tetrahedron Lett.*, 2001, **42**, 1441–1443.
54 X. Li, D. T. Moore and S. S. Iyengar, *J. Chem. Phys.*, 2008, **128**, 184308.
55 N. I. Hammer, E. G. Diken, J. R. Roscioli, M. A. Johnson, E. M. Myshakin, K. D. Jordan, A. B. McCoy, X. Huang, J. M. Bowman and S. Carter, *J. Chem. Phys.*, 2005, **122**, 244301.